

## Band-gap scaling of graphene nanohole superlattices

Wei Liu,<sup>1,2</sup> Z. F. Wang,<sup>2</sup> Q. W. Shi,<sup>1</sup> Jinlong Yang,<sup>1</sup> and Feng Liu<sup>2</sup>

<sup>1</sup>Hefei National Laboratory for Physical Sciences at Microscale, University of Science and Technology of China, Hefei, Anhui 230026, China

<sup>2</sup>Department of Materials Science and Engineering, University of Utah, Salt Lake City, Utah 84112, USA  
(Received 5 October 2009; revised manuscript received 13 November 2009; published 11 December 2009)

Based on the tight-binding model, we investigate band structures of graphene nanohole (GNH) superlattices as a function of NH size and density. One common origin of band gaps for GNH superlattices with NHs of either armchair or zigzag edges is the quantum-confinement effect due to the periodic potential introduced by the NHs, which turns the semimetallic sheet into a direct-gap semiconductor. Additional band gaps also open for GNH superlattices with NHs of zigzag edges in a ferromagnetic ground state, arising from the staggered sublattice potential on the zigzag edges due to edge magnetization. Our calculations reveal a generic scaling relation that both types of band gaps increase linearly with the product of NH size and density.

DOI: [10.1103/PhysRevB.80.233405](https://doi.org/10.1103/PhysRevB.80.233405)

PACS number(s): 73.22.-f, 72.80.Rj, 75.70.Ak

The electronic structure of nanoscale carbon materials such as fullerenes and carbon nanotubes has been intensively studied during the past two decades.<sup>1</sup> Among the carbon materials, graphene is a rapidly rising star showing a wealth of interesting unconventional electronic properties and a broad range of potential applications.<sup>2</sup> In addition to two-dimensional (2D) graphene sheet, much attention has also been drawn to graphene-based low-dimensional nanostructures such as zero-dimensional nanodots<sup>3-5</sup> and nanoholes (antidots),<sup>6-9</sup> one-dimensional nanoribbons,<sup>10-16</sup> as well as 2D graphene nanohole superlattices.<sup>6-8</sup> These structures exhibit unique electronic structures different from the graphene sheet itself and hence offering other application potentials.

There are two key effects in determining the electronic properties of these low-dimensional graphene nanostructures: the size effect and edge effect, the former induces quantum confinement converting the semimetallic graphene into semiconductors and the latter induces edge magnetism as well as opening a small band gap. Both these effects have been extensively studied in graphene nanoribbons and show strong size and shape dependences.<sup>10-16</sup> For example, it has been shown that the band gap of nanoribbons scales inversely with their width<sup>10-12</sup> and nanoribbons with zigzag edges may have either a ferromagnetic (FM) or antiferromagnetic (AFM) ground state depending on their edge orientations.<sup>8,10,16</sup> On the other hand, less studies have been done for 2D GNH superlattices. Pedersen *et al.*<sup>7</sup> showed a linear scaling of the band gaps for circular GNH superlattice. However, it has been recently observed that graphene edges are generally straight stabilized with either armchair or zigzag edges.<sup>17,18</sup> Motivated by these new experiments, we have carried out tight-binding (TB) calculations and theoretical analyses to investigate the relationship between the band gap and the nanohole size/density for GNH superlattices with armchair and zigzag edges.

Our numerical calculations show that both the armchair- and zigzag-edged triangular GNH (TGNH) and rhombus GNH (RGNH) superlattices have nonzero and direct band gaps. The band gaps of armchair GNH superlattice originate solely from the quantum-confinement effect of 2D periodic potential created by the NHs. While for zigzag GNH superlattices, two types of band gaps arise, one from the periodic

potential and the other from the staggered sublattice potential due to spin-ordered states at the zigzag edges. A generic scaling rule is found that both types of band gaps increase linearly with the product of NH size and density.

We have studied TGNH and RGNH superlattices with armchair and zigzag edges for different NH size and density (i.e., unit-cell size), as illustrated in Fig. 1. We denote a given superlattice structure by two integers: the hole side length  $l$  and unit-cell side length  $L$ , as  $l@L$ , in the length unit of  $a$  and  $\sqrt{3}a$  for armchair and zigzag NH, respectively. Here  $a=1.42$  Å is C-C bond length. Much of the electronic and transport properties of graphene-based materials can be understood starting from a one-parameter, nearest-neighbor,  $\pi$ -orbital TB model, which could accurately reproduce the low-energy density-functional results of graphene.<sup>10</sup> We have modeled the armchair GNH superlattices using the one-parameter TB Hamiltonian as

$$H_0 = \gamma \sum_{\langle i,j \rangle, \sigma} c_{i\sigma}^\dagger c_{j\sigma}, \quad (1)$$

where  $c_{i\sigma}^\dagger$  and  $c_{i\sigma}$  are, respectively, creation and annihilation operators for an electron of spin  $\sigma$  in the  $\pi$  orbital centered

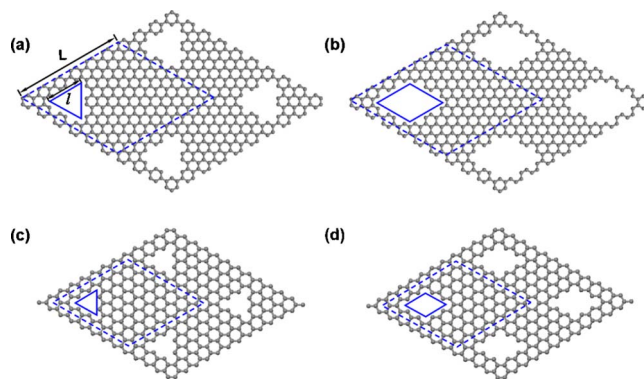


FIG. 1. (Color online) Schematics of GNH superlattices: (a) 6@18 armchair TGNH. (b) 6@18 armchair RGNH. (c) 2@7 zigzag TGNH. (d) 2@7 zigzag RGNH. The gray balls are carbon atoms. The solid and dashed blue lines denote the side length of NH ( $l$ ) and unit cell ( $L$ ), respectively.

on the  $i$ th carbon atom, and  $\gamma = -2.6$  eV is the nearest-neighbor hopping integral. In this description, energy levels are always distributed symmetrically above and below Fermi level at zero energy in the undoped case.

The one-parameter TB model, however, does not incorporate the essential ingredients necessary to reproduce the spin polarization for zigzag edges in graphene found in density-functional theory (DFT) calculations.<sup>10</sup> In order to describe the spin effect in zigzag GNH superlattices, we then adopt a two-parameter TB Hamiltonian as<sup>19,20</sup>

$$H_0 = \gamma \sum_{(i,j),\sigma} c_{i\sigma}^+ c_{j\sigma} + U \sum_{i,\sigma} (\langle n_{i,-\sigma} \rangle - 1/2) n_{i\sigma}, \quad (2)$$

where  $n_{i\sigma}$  is the number operator, and  $U = 2.75$  eV is parameterized from the spin-unrestricted local-density-functional results. This additional parameter  $U$  is necessary because the localized edge states (present in zigzag edges but absent in armchair edges) enhance the effects of electron-electron interactions at the zigzag edges.  $n_{i\uparrow,\downarrow}$  is computed self-consistently from

$$\langle n_{i\sigma} \rangle = \int_{-\infty}^{E_f} dE g_{i\sigma}(E), \quad (3)$$

where  $E_f = 0$  is the Fermi energy and  $g_{i\sigma}$  is local spin density of states obtained from Eq. (2). Equations (2) and (3) must be solved self-consistently, which is equivalent to those found from a Hartree-Fock approximation to the Hubbard model. Recently, Fürst *et al.*<sup>21</sup> have shown that the TB model agrees well with DFT for calculations performed on graphene antidot lattices.

We first present the calculated electronic band structures of armchair TGNH and RGNH superlattices. The energy bands of 6@18 armchair TGNH and RGNH superlattices are shown in Figs. 2(a) and 2(b), respectively. Different from pristine graphene, a substantial band gap,  $E_g = 0.435$  eV for TGNH and  $E_g = 0.138$  eV for RGNH, opens up at the Fermi level. The origin of band gap is due to the periodic perturbation potential created by NHs, which turns the semimetallic sheet into a direct-gap semiconductor. Similar behaviors have also been discussed for the circular GNH superlattices<sup>7</sup> and graphene under periodic potentials.<sup>22</sup>

Next, we present the band structures of zigzag TGNH and RGNH superlattices. The energy bands of 5@10 zigzag TGNH and 5@10 zigzag RGNH superlattices are shown in Figs. 2(c) and 2(d), respectively. The nanohole shape plays an important role in determining the electronic properties of GNH superlattices.<sup>23</sup> In a nonspin state, zigzag edge would produce a dispersionless metallic band at the Fermi level. Its bandwidth is identically zero as predicted in the one-parameter nearest-neighbor TB model. However, in the spin-polarized state as predicted in the two-parameter TB model, the dispersionless metallic band splits into multiple subbands. As discussed in Yu's work,<sup>8</sup> spins are parallel (FM coupling) on all the zigzag edges which are at angles of  $0^\circ$  and  $120^\circ$  to each other, and antiparallel (AFM coupling) at angles of  $60^\circ$  and  $180^\circ$ . Consequently, the ground state of the zigzag TGNH is FM while that of the zigzag RGNH is AFM.<sup>8</sup> Furthermore, the spin polarization opens a spin-

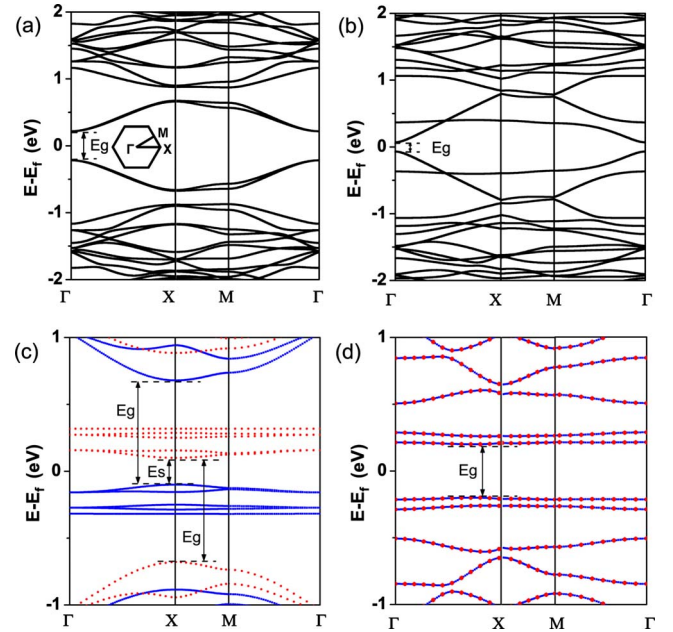


FIG. 2. (Color online) Band structures of GNH superlattices. (a) 6@18 armchair TGNH superlattice, the inset shows the first Brillouin zone with the three high-symmetry axes indicated, along which the band structure was calculated. (b) 6@18 armchair RGNH superlattice. (c) 5@10 zigzag TGNH superlattice, red dot and blue line denote spin-up and -down bands in the FM ground state;  $E_g$  and  $E_s$  are the band gap and spin-splitting gap, respectively. (d) 5@10 zigzag RGNH superlattice, spin bands are degenerate in the AFM ground state.

splitting gap ( $E_s$ ) in addition to the quantum-confinement gap ( $E_g$ ) induced by the periodic NH potential. For the FM 5@10 zigzag TGNH superlattice [Fig. 2(c)],  $E_g = 0.779$  eV for both the spin-up and spin-down bands, and  $E_s = 0.2$  eV between the spin-up and spin-down bands. For the AFM 5@10 RGNH superlattice [Fig. 2(d)],  $E_g = 0.4$  eV and  $E_s = 0.0$  eV. The spin-splitting gap originates from the staggered sublattice potential at the zigzag edges due to the edge magnetization. We found that the number of split subbands for spin-up and spin-down is the same, which is determined by  $N_A - N_B$ , and  $N_A(N_B)$  is the number of removed carbon atoms  $A(B)$  in the unit cell (graphene consists of two atomic sublattices of  $A$  and  $B$ ). This is consistent with Lieb's theorem<sup>24</sup> of the ground-state spin configuration on a bipartite lattice.<sup>6,8,25</sup> For the FM 5@10 zigzag TGNH, 25 atoms are removed from the unit cell, and among them 15 atoms belong to the  $A$  site and 10 belong to the  $B$  site. Consequently, both spin-up and spin-down bands split into five subbands and a finite spin-splitting gap ( $E_s$ ) opens up, as shown in Fig. 2(c).

In contrast, the zigzag RGNH superlattices have an AFM ground state<sup>8</sup> so that the spin-up band is energy degenerate with the spin-down band with a zero spin-splitting gap ( $E_s$ ), as shown in Fig. 2(d). In general, two kinds of band gaps of FM zigzag GNH superlattices arise from a combined effect of NH periodic perturbation and the edge magnetization.

The band gaps of GNH superlattices are expected to depend on NH size and density (or unit-cell size). To reveal such dependence, we have calculated the band gaps for all

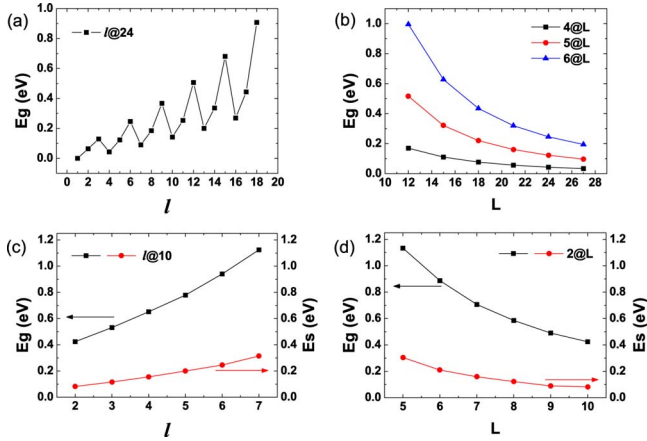


FIG. 3. (Color online) Armchair TGNH superlattices: (a) Band gap vs NH side length with  $L=24$ . (b) Band gap vs unit-cell side length with  $l=4, 5, 6$ . Zigzag TGNH superlattices. (c) Band gap and spin-splitting gap vs NH side length with  $L=10$ . (d) Band gap and spin-splitting gap vs unit-cell side length with  $l=2$ .

four types of GNH superlattices as a function of NH side length ( $l$ ) at the fixed unit-cell side length ( $L$ ), and as a function of  $L$  at the fixed  $l$ . The results are shown in Figs. 3 and 4 for TGNH and RGNH superlattices, respectively. For armchair TGNH superlattices, one notices that the band gap displays an oscillatory increase with the increasing NH side length  $l$  at the fixed cell side length  $L$ , with a period of three [Fig. 3(a)]. This behavior is qualitatively the same as the band gap of armchair graphene nanoribbons depending on their width.<sup>10–12</sup> The physical origin of the oscillation arises from the different matching relationships between the wave vectors of the confined states with the Fermi vector of graphene. For the same reason, at the fixed NH side length  $l$ , there are three branches of band gaps corresponding to different  $l$  as a function of cell side length  $L$ ; the gap in each  $l$  branch decreases monotonically with increasing  $L$

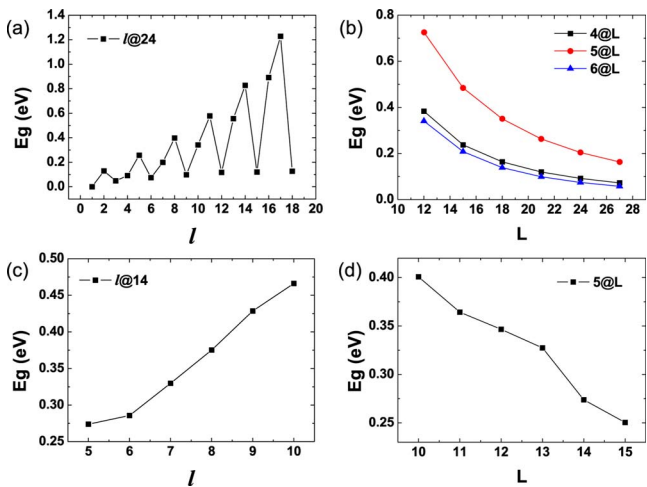


FIG. 4. (Color online) Armchair RGNH superlattices: (a) Band gap vs NH side length with  $L=24$ . (b) Band gap vs unit-cell side length with  $l=4, 5, 6$ . Zigzag RGNH superlattices. (c) Band gap vs NH side length with  $L=14$ . (d) Band gap vs unit-cell side length with  $l=5$ .

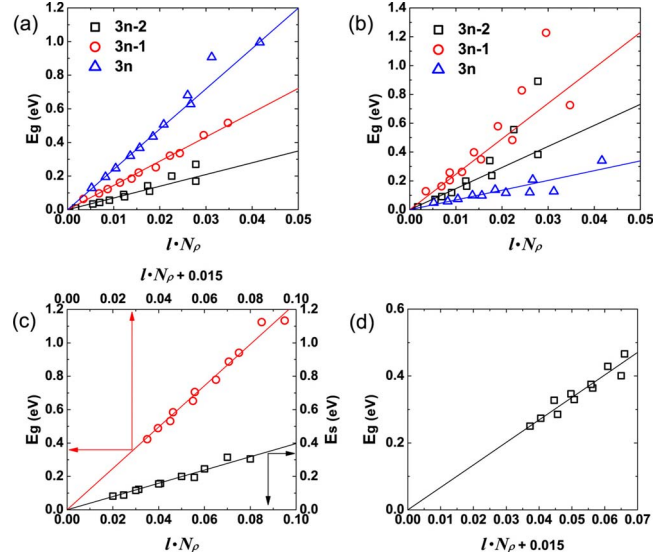


FIG. 5. (Color online) (a) and (b) are band-gap scaling for armchair TGNH and RGNH superlattices. (c) and (d) are band-gap and spin-splitting gap scaling for zigzag TGNH and RGNH superlattices. Square, triangle, and circle dots are the TB results, colored lines are the linear fitting curves for the band gaps. Fitting constant  $\lambda$  is listed in Table I.

[Fig. 3(b)]. For zigzag TGNH superlattices, the wave vector of one confined state always matches with the Fermi vector of graphene inducing a localized state at the Fermi energy so that there will be no oscillatory behavior in band gap as a function of NH size. However, this localized state at Fermi energy induces an instability against spin polarization, which opens up a spin-splitting gap ( $E_s$ ) in addition to the quantum-confinement gap ( $E_g$ ). Our calculations show that both  $E_g$  and  $E_s$  increase monotonically with the increasing  $l$  at the fixed  $L$  [Fig. 3(c)], and decrease monotonically with the increasing  $L$  at the fixed  $l$  [Fig. 3(d)]. The band gap of RGNH superlattices behave qualitatively in the same way as those of TGNH superlattices (comparing Fig. 4 to Fig. 3), except that the zigzag RGNH superlattices have an AFM ground state so that their  $E_s$  is always zero.

Effectively, we may consider the GNH superlattices consist of a 2D network of crossing nanoribbons. Then, in general, the quantum-confinement band gap  $E_g$  is expected to increase with the decreasing nanoribbon width due to stronger confinement, and the nanoribbon width can be decreased by either increasing NH side length  $l$  at the fixed cell side length  $L$  or decreasing cell side length  $L$  at the fixed NH side length  $l$ , leading to the results shown in Figs. 3 and 4. Also, a smaller nanoribbon width also makes the spin-splitting gap  $E_s$  larger for the zigzag TGNH superlattices [Figs. 3(c) and 3(d)] because the smaller width gives rise to a larger perturbation to the staggered zigzag-edge potentials which makes the energy difference between the spin-up and spin-down states larger.

Recently, Pedersen *et al.*<sup>7</sup> have shown a simple scaling rule for the band gaps of circular GNH superlattices which scale with the NH size and density as  $E_g = \lambda \times f(lN_\rho)$ , where  $N_\rho = 1/L^2$  is the number of NHs per area, i.e., the NH number density. Here, we have tested this scaling rule for different

TABLE I. Fitting parameter  $\lambda$ .

| $\lambda$ (eV) | $E_g$  |        |       | $E_s$ |
|----------------|--------|--------|-------|-------|
| $l$            | $3n-2$ | $3n-1$ | $3n$  |       |
| Armchair TGNH  | 6.99   | 14.42  | 23.97 |       |
| Armchair RGNH  | 14.63  | 24.59  | 6.78  |       |
| Zigzag TGNH    |        | 12.39  |       | 3.97  |
| Zigzag RGNH    |        | 6.72   |       |       |

NH shapes and edges in TGNH and RGNH superlattices as well as for spin-splitting gaps in addition to quantum-confinement gaps. Figure 5 shows that all of the calculated TB results can be nicely fitted by the same scaling rule when  $lN_\rho$  is small, especially at the limit of small NH size and/or small NH density. (At large hole size and/or higher hole density, there can be stronger interactions between the crossing network of ribbons. Note that without interribbon interaction, the similar scaling law applies to a single nanoribbon for all sizes.) This indicates that this simple scaling rule is generally applicable to different NH shapes and to both types of band gaps. Specifically, from the linear fitting of the calculated data we obtain the following fitting constants. For armchair TGNH and RGNH superlattices, different scaling components (i.e., fitting parameters  $\lambda$  listed in Table I) exist for the three different NH branches, as shown in Figs. 4(a)

and 4(b), respectively. For zigzag TGNH and RGNH superlattices,  $f \propto lN_\rho + 0.015$  is used for scaling the quantum-confinement gaps ( $E_g$ ), and  $f \propto lN_\rho$  for scaling the spin-splitting gaps ( $E_s$ ). The small quantity 0.015 is added to ensure the fitting curves of  $E_g$  passing through the zero point so that the band gap goes to zero at the limit of pristine graphene as required. Again, different scaling components exist for different hole types and lattice symmetries, as listed in Table I.

In summary, we have theoretically studied the band-gap formation of TGNH and RGNH superlattices with armchair and zigzag NH edges. A common quantum-confinement band gap opens up in all types of superlattices due to the finite-size effect of nanoribbon crossing network. In addition, a spin-splitting gap opens up in the zigzag TGNH superlattices with a FM ground state. A generic scaling rule is established for both types of band gaps and for all the NH superlattices: the band gap increases linearly with the increasing product of NH size and density at the limit of small NH size and/or density. This simple scaling rule can be useful in the future design of GNH superlattices for their potential applications in graphene-based nanoelectronic and spintronics.

This work is supported by DOE. We thank DOE-NERSC and Center for High Performance Computing (CHPC) at the University of Utah for providing the computing resources.

- <sup>1</sup>M. S. Dresselhaus, G. Dresselhaus, and P. C. Eklund, *Science of Fullerenes and Carbon Nanotubes: Their Properties and Applications* (Academic, New York, 1996).
- <sup>2</sup>A. K. Geim and K. S. Novoselov, *Nature Mater.* **6**, 183 (2007).
- <sup>3</sup>J. Fernández-Rossier and J. J. Palacios, *Phys. Rev. Lett.* **99**, 177204 (2007).
- <sup>4</sup>W. L. Wang, S. Meng, and E. Kaxiras, *Nano Lett.* **8**, 241 (2008).
- <sup>5</sup>O. Hod, V. Barone, and G. E. Scuseria, *Phys. Rev. B* **77**, 035411 (2008).
- <sup>6</sup>D. Yu, E. M. Lupton, M. Liu, W. Liu, and F. Liu, *Nano Res.* **1**, 56 (2008).
- <sup>7</sup>T. G. Pedersen, C. Flindt, J. Pedersen, N. A. Mortensen, A.-P. Jauho, and K. Pedersen, *Phys. Rev. Lett.* **100**, 136804 (2008).
- <sup>8</sup>D. Yu, E. M. Lupton, H. J. Gao, C. Zhang, and F. Liu, *Nano Res.* **1**, 497 (2008).
- <sup>9</sup>X. H. Zheng, G. R. Zhang, Z. Zeng, V. M. García-Suárez, and C. J. Lambert, *Phys. Rev. B* **80**, 075413 (2009).
- <sup>10</sup>Y.-W. Son, M. L. Cohen, and S. G. Louie, *Phys. Rev. Lett.* **97**, 216803 (2006).
- <sup>11</sup>Q. Yan, B. Huang, J. Yu, F. Zheng, J. Zang, J. Wu, B.-L. Gu, F. Liu, and W. Duan, *Nano Lett.* **7**, 1469 (2007).
- <sup>12</sup>Z. F. Wang, Q. Li, H. Zheng, H. Ren, H. Su, Q. W. Shi, and J. Chen, *Phys. Rev. B* **75**, 113406 (2007).
- <sup>13</sup>H. Zheng, Z. F. Wang, T. Luo, Q. W. Shi, and J. Chen, *Phys. Rev. B* **75**, 165414 (2007).
- <sup>14</sup>E. Kan, Z. Li, J. Yang, and J. G. Hou, *J. Am. Chem. Soc.* **130**, 4224 (2008).
- <sup>15</sup>B. Huang, F. Liu, J. Wu, B.-L. Gu, and W. Duan, *Phys. Rev. B* **77**, 153411 (2008).
- <sup>16</sup>X. Wu and X. C. Zeng, *Nano Res.* **1**, 40 (2008).
- <sup>17</sup>X. Jia, M. Hofmann, V. Meunier, B. G. Sumpter, J. Campos-Delgado, J. M. Romo-Herrera, H. Son, Y.-P. Hsieh, A. Reina, J. Kong, M. Terrones, and M. S. Dresselhaus, *Science* **323**, 1701 (2009).
- <sup>18</sup>Ç. Ö. Girit, J. C. Meyer, R. Ermi, M. D. Rossell, C. Kisielowski, L. Yang, C.-H. Park, M. F. Crommie, M. L. Cohen, S. G. Louie, and A. Zettl, *Science* **323**, 1705 (2009).
- <sup>19</sup>D. Gunlycke, D. A. Areshkin, J. Li, J. W. Mintmire, and C. T. White, *Nano Lett.* **7**, 3608 (2007).
- <sup>20</sup>J. Guo, D. Gunlycke, and C. T. White, *Appl. Phys. Lett.* **92**, 163109 (2008).
- <sup>21</sup>J. A. Fürst, J. G. Pedersen, C. Flindt, N. A. Mortensen, M. Brandbyge, T. G. Pedersen, and A.-P. Jauho, *New J. Phys.* **11**, 095020 (2009).
- <sup>22</sup>C.-H. Park, L. Yang, Y.-W. Son, M. L. Cohen, and S. G. Louie, *Nat. Phys.* **4**, 213 (2008).
- <sup>23</sup>T. G. Pedersen, C. Flindt, J. Pedersen, A.-P. Jauho, N. A. Mortensen, and K. Pedersen, *Phys. Rev. B* **77**, 245431 (2008).
- <sup>24</sup>E. H. Lieb, *Phys. Rev. Lett.* **62**, 1201 (1989).
- <sup>25</sup>M. Vanević, V. M. Stojanović, and M. Kindermann, *Phys. Rev. B* **80**, 045410 (2009).